

Correlation Effects in Orbital Magnetism

T. J. Sjöstrand,¹ K. Karlsson,² and F. Aryasetiawan¹

¹*Department of Physics, Division of Mathematical Physics,
Lund University, Professorgatan 1, 223 62 Lund, Sweden*

²*Department of Engineering Sciences, University of Skövde, SE-541 28 Skövde, Sweden*
(Dated: May 28, 2019)

Orbital magnetization is known empirically to play an important role in several magnetic phenomena, such as permanent magnetism and ferromagnetic superconductivity. Within the recently developed "modern theory of orbital magnetization", theoretical insight has been gained into the nature of this often neglected contribution to magnetism, but is based on an underlying mean-field approximation. From this theory, a few treatments have emerged which also take into account correlations beyond the mean-field approximation. Here, we apply the scheme developed in a previous work [Phys. Rev. B **93**, 161104(R) (2016)] to the Haldane-Hubbard model to investigate the effect of charge fluctuations on the orbital magnetization within the *GW* approximation. Qualitatively, we are led to distinguish between two quite different situations: (i) When the lattice potential is larger than the nearest neighbor hopping, the correlations are found to boost the orbital magnetization. (ii) If the nearest neighbor hopping is instead larger than the lattice potential, the correlations reduce the magnetization.

PACS numbers: 71.20.-b, 71.27.+a

I. INTRODUCTION

Magnetism is usually associated with the spin of the electrons since the magnetic moment arising from the orbital motion of the electrons is normally weak or even completely quenched crystals with time-reversal symmetry. However, the role of the orbital motion in determining magnetic properties is not to be underestimated. Magnetic anisotropy, which is important in permanent magnets, has its roots in the orbital magnetic moment.¹⁻³ Magnetic susceptibility,⁴ magnetoelectric response⁵⁻⁷ and spin-dependent transport^{4,8-10} can also be strongly influenced by it. Recent experiments on ferromagnetic superconductors show the possibility of the orbital moment dominating over the spin counterpart.¹¹ This is particularly notable as the two appear with opposite signs and tend to cancel each other.

The orbital magnetic moment in a crystal has two contributions: one arising from the local atomic orbital moments and, less obvious, a contribution from the itinerant edge states on the surface of the crystal, which in the thermodynamic limit can be expressed solely as bulk quantities.¹²⁻¹⁵ Computing the orbital magnetization in infinite crystals has long been recognized to be nontrivial due to the position operator being ill-defined in the extended Bloch basis.^{16,17} Not long ago, the so called *modern* theory of orbital magnetization was established,¹⁸⁻²¹ where the orbital magnetization was expressed as a true bulk quantity evaluated from the extended Bloch states. These pioneering works have opened up a way for computing the orbital magnetic moment from realistic band structure calculations,^{22,23} usually obtained from Kohn-Sham density functional theory.

An interesting application of the modern theory is to materials where the electrons responsible for the orbital magnetization are semi-itinerant. A well-known example

is iron, which, contrary to nickel and cobalt, has a large itinerant contribution coming from the *3d* electrons. Recently, Hanke *et al.*²⁴ applied the theory to a variety of structural inhomogeneous systems, including topological ferromagnets. Several prototypical insulating perovskite transition metal oxides have also been studied.²⁵ Magnetic thin films,²⁶ non-collinear spin systems and frustrated spin lattices are additional candidates with spintronics applications.^{27,28}

The modern mean-field theory is not expected to yield physically meaningful results for moderately to strongly correlated materials. Even in the ferromagnetic transition metals, the orbital moment is known to be underestimated when performing density functional calculations using the gradient corrected PBE functional.²³ Systematic improvement of the calculation of the orbital magnetization in correlated systems is particularly crucial when the desired physical quantity depends on the balance between the orbital and spin magnetization. An important example is the compensation temperature of zero-magnetization ferromagnets, at which the spin and orbital magnetization exactly cancel out.

Extensions have been formulated within current and spin density functional theory,¹⁹ but also in terms of the full Green's function and vertex function.²⁹ Recently, we have derived a formula from *first principles* for the orbital magnetic moment of interacting electrons.^{30,31} The formula factorizes into two parts, one that contains the information about the one-particle band structure and another that contains the effect of exchange and correlations beyond the local density approximation, carried by the Green's function. The self-energy, which determines the Green's function via Dyson's equation, can be calculated using the *GW* approximation³² for weakly to moderately correlated materials and the LDA+DMFT³³ or *GW*+DMFT³⁴ approximations for strongly correlated

arXiv:1905.1143v1 [cond-mat.str-el] 27 May 2019

materials.

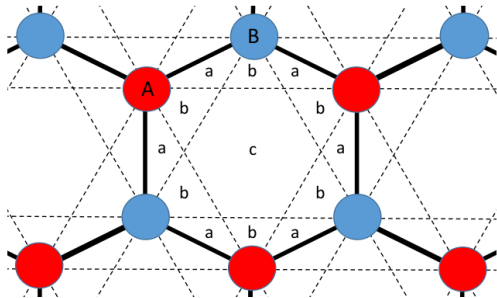


FIG. 1. The honeycomb lattice with two different (A and B) atoms per unit cell. The fluxes in regions a , b and c obey $\varphi_a = -\varphi_b$ and $\varphi_c = 0$. This implies that the total flux in the unit cell is zero. The flux φ in Eq. (1) is defined as $\varphi = 2\varphi_a + \varphi_b$. The figure is from Ref. 30.

Here, we apply our previously derived Green's function formula for the orbital magnetization to the 2D Haldane-Hubbard model within the GW approximation, as a first step to understand the effect of correlations on the magnetization in real systems. In Sec. II we briefly describe the essentials of the Haldane-Hubbard model. In Sec. III we revisit the - until now - untested Green's function formula and summarize the approximations and computational details of this work. We present the results within the GW and Hartree-Fock approximations in Sec. IV for different values of the parameters of the model. The main findings are discussed in Sec. V.

II. THE 2D HALDANE-HUBBARD MODEL

The famous 2D Haldane model³⁵ has been used for decades in studies of topologically non-trivial systems, such as Chern insulators and Z_2 topological insulators.³⁶ The Haldane model mimics the quantum Hall effect³⁷ with a time-reversal breaking internal microscopic field which averages to zero in the unit cell. Recently, the Haldane model was experimentally realized by using ultra-cold atoms.³⁸

In the non-interacting Haldane model the Hamiltonian is expressed as

$$\begin{aligned} \hat{H}_0 = & -t_1 \sum_{i\sigma} [a_{i\sigma}^\dagger b_{i+\delta_1\sigma} + a_{i\sigma}^\dagger b_{i+\delta_2\sigma} + a_{i\sigma}^\dagger b_{i+\delta_3\sigma} + \text{h.c.}] \\ & -t_2 (e^{i\varphi} \sum_{i\sigma} [a_{i\sigma}^\dagger a_{i+\nu_1\sigma} + a_{i+\nu_1\sigma}^\dagger a_{i-\nu_2\sigma} + a_{i-\nu_2\sigma}^\dagger a_{i\sigma}]) \\ & + \text{h.c.} + [\varphi \rightarrow -\varphi, a \rightarrow b] + \Delta_{AB} \sum_{i\sigma} [a_{i\sigma}^\dagger a_{i\sigma} - b_{i\sigma}^\dagger b_{i\sigma}], \end{aligned} \quad (1)$$

The annihilation operators $a_{i\sigma}$ belong to sublattice A and $b_{i\sigma}$ to sublattice B. We restrict our study to having two electrons per unit cell, which results in one fully occupied and one empty band. t_1 is the real nearest-neighbor hopping between sublattices A and B of the

honeycomb lattice. With lattice constant $a = 1$, the nearest neighbor vectors are $\delta_1 = (0, 1)$, $\delta_2 = (-\frac{\sqrt{3}}{2}, \frac{1}{2})$ and $\delta_3 = (\frac{\sqrt{3}}{2}, \frac{1}{2})$, see Fig. 1. The next-nearest neighbor vectors that explicitly enter the Hamiltonian are $\nu_1 = (\sqrt{3}, 0)$ and $\nu_2 = (\frac{\sqrt{3}}{2}, -\frac{3}{2})$. t_2 and φ denote the amplitude and complex phase of the next-nearest neighbor hopping. φ mimics a microscopic magnetic field which breaks time-reversal symmetry if it differs from a multiple of π . The magnetic flux, by construction, averages to zero in the unit cell. Δ_{AB} models a staggered potential between the two sublattices and breaks the inversion symmetry and gives mass to the Dirac fermions. Pure graphene has $\Delta_{AB} = 0$ whereas epitaxial graphene has a non-vanishing Δ_{AB} (see e.g. Ref. 39). The possibility of tuning the band gap in graphene by doping makes way for a wider range of technological applications, e.g. logic gates. The effect of this doping is beautifully captured by the Haldane model, but it is also ideal for describing several insulators, with a larger value of Δ_{AB} , such as two-dimensional hexagonal boron nitride.

The Hall conductance σ_{xy} is given by an integer C , called the Chern number, times e^2/h . C is an intrinsic property of the band structure, given by

$$C = \frac{i}{2\pi} \sum_n \int_{BZ} \frac{d\mathbf{q}}{(2\pi)^2} \left[\left\langle \frac{\partial u_{n\mathbf{q}}}{\partial q_x} \middle| \frac{\partial u_{n\mathbf{q}}}{\partial q_y} \right\rangle - \left\langle \frac{\partial u_{n\mathbf{q}}}{\partial q_y} \middle| \frac{\partial u_{n\mathbf{q}}}{\partial q_x} \right\rangle \right], \quad (2)$$

for periodic 2D systems, where $|u_{n\mathbf{q}}\rangle = e^{-i\mathbf{q}\cdot\mathbf{r}}|\psi_{n\mathbf{q}}\rangle$ are the Bloch-periodic functions. Note that C is independent of the gauge chosen for $|u_{n\mathbf{q}}\rangle$. This formula is also valid when including correlations, but $|u_{n\mathbf{q}}\rangle$ will then contain additional information, as discussed in the next section. The phase transitions where C changes are always accompanied by the closing and reopening of the band gap.

The total Hamiltonian, $\hat{H} = \hat{H}_0 + \hat{V}_{e-e}$, also contains the electron-electron interaction term

$$\hat{V}_{e-e} = \frac{1}{2} \sum_{ijkl, \sigma\sigma'} U_{ijkl} c_{i\sigma}^\dagger c_{j\sigma'}^\dagger c_{l\sigma'} c_{k\sigma}, \quad (3)$$

where $c_i = a_i$ or $c_i = b_i$ if i corresponds to sublattice A or B, respectively, and

$$U_{ijkl} = \int d\mathbf{r}d\mathbf{r}' \frac{\phi_i^*(\mathbf{r})\phi_j^*(\mathbf{r}')\phi_l(\mathbf{r}')\phi_k(\mathbf{r})}{|\mathbf{r} - \mathbf{r}'|}. \quad (4)$$

In this work, the orbitals ϕ_i are assumed to be localized and only the short-ranged direct Coulomb integrals $U = U_{iiii}$ and $U' = U_{ijij}$ are kept, where i and j are nearest neighbor sites. U is the on-site interaction of the Hubbard model and U' is the nearest-neighbor interaction. We intend to go beyond this approximation in a future study on real materials by including more Coulomb integrals, in particular exchange integrals U_{ijji} , all calculated using the constrained random-phase approximation.⁴⁰ Indeed, this approximation has already been applied to graphene, see Ref. 41.

III. CORRELATIONS AND ORBITAL MAGNETIZATION

A. Exact Expressions

The expression for the orbital magnetization, M_{orb} , derived in Ref. 31, is readily generalized to electrons with

$$M_z^L = \sum_{jk,nn'} \epsilon_{zjk} \int_{BZ} \frac{d\mathbf{q}}{(2\pi)^2} \left[G_{n'n}^+(\mathbf{q}) \left\langle \frac{\partial u_{n\mathbf{q}}}{\partial q_j} \middle| H(\mathbf{q}) - \mu \left| \frac{\partial u_{n'\mathbf{q}}}{\partial q_k} \right\rangle + \frac{\partial G_{n'n}^+(\mathbf{q})}{\partial q_k} \left\langle \frac{\partial u_{n\mathbf{q}}}{\partial q_j} \middle| u_{n'\mathbf{q}} \right\rangle (E_{n'\mathbf{q}} - \mu) \right], \quad (5)$$

$$M_z^I = \sum_{jk,nn'} \epsilon_{zjk} \int_{BZ} \frac{d\mathbf{q}}{(2\pi)^2} G_{n'n}^+(\mathbf{q}) \left[\left\langle \frac{\partial u_{n\mathbf{q}}}{\partial q_j} \middle| \frac{\partial u_{n'\mathbf{q}}}{\partial q_k} \right\rangle (E_{n'\mathbf{q}} - \mu) + \frac{\partial E_{n\mathbf{q}}^0}{\partial q_j} \left\langle \frac{\partial u_{n\mathbf{q}}}{\partial q_k} \middle| u_{n'\mathbf{q}} \right\rangle \right]. \quad (6)$$

The orbital magnetic moment is obtained by multiplying with the factor $-e/2c$, in Gaussian units. The sums are over *all* bands n and n' . μ denotes the chemical potential and ϵ_{ijk} the Levi-Civita symbol, where ijk are cartesian indices and, in particular, z is perpendicular to the 2D plane. The spin index has been left out for simplicity. More precisely, $H(\mathbf{q}) = e^{-i\mathbf{q}\cdot\mathbf{r}} H e^{i\mathbf{q}\cdot\mathbf{r}}$ with $H(\mathbf{q})|u_{n\mathbf{q}}\rangle = E_{n\mathbf{q}}|u_{n\mathbf{q}}\rangle$ where the one-particle Hamiltonian H is defined from

$$\hat{H}_{\text{MF}} = \sum_{\sigma} \int d\mathbf{r} \psi_{\sigma}^{\dagger}(\mathbf{r}) H(\mathbf{r}) \psi_{\sigma}(\mathbf{r}). \quad (7)$$

Here, \hat{H}_{MF} is the self-consistent mean field of $\hat{H}_0 + \hat{V}_{e-e}$.

The central quantities for the calculation of M_{orb} are the band-index matrix elements of the one-particle Green's function,

$$G_{nn'}^+(\mathbf{q}) = \lim_{\eta \rightarrow 0^+} \int \frac{d\omega}{2\pi} G_{nn'}(\mathbf{q}; \omega) e^{i\omega\eta}, \quad (8)$$

$$[G^{-1}]_{nn'}(\mathbf{q}; \omega) = [g^{-1}]_{nn}(\mathbf{q}; \omega) \delta_{nn'} - \Sigma_{nn'}(\mathbf{q}; \omega). \quad (9)$$

The Hartree-potential is contained in the mean-field Green's function, g , whereas the self-energy $\Sigma = \Sigma^x + \Sigma^c$ contains all effects from exchange and correlations. The Chern number for the correlated system is obtained by defining $|u_{n\mathbf{k}}\rangle$ from the diagonalization of $-G^{-1}(\mathbf{q}; 0) = H(\mathbf{q}) + \Sigma(\mathbf{q}; 0)$.⁴² The model contains only one orbital per lattice site, so the exchange vanishes when the Coulomb interaction is approximated by the on-site U . Since we assume localized orbitals, the exchange between different sites also vanishes, implying that $\Sigma^x = 0$.

The main purpose of this paper is to study electron correlation effects in the context of orbital magnetization. We compare M_{orb} within (a) the Hartree-Fock approximation and (b) the GW approximation, for a range of value of the Coulomb integrals, U and U' .

spin when spin-orbit interaction is neglected. For spin-independent systems, like that described by Eq. (1), the contributions to M_{orb} from spin \uparrow and \downarrow are the same. We adopt the notation that the orbital magnetization in one spin channel is M_{orb} .

The orbital magnetization is perpendicular to the 2D plane of the Haldane model and is a sum of a local and an itinerant contribution:

B. Approximating G

(a) Hartree-Fock approximation: This amounts to neglecting correlations, $\Sigma^c = 0$. Since also $\Sigma^x = 0$, this is identical to the Hartree approximation, so we can write $g(\mathbf{q}; \omega) = (\omega - H(\mathbf{q}))^{-1}$.

(b) GW approximation:

$$\Sigma_{nn'}^c(\mathbf{q}; \omega) = i \sum_{km} \int \frac{d\omega'}{2\pi} [g_{mm}(\mathbf{k}; \omega + \omega')] \times \langle \psi_{n\mathbf{q}} \psi_{m\mathbf{k}} | W^c(\omega') | \psi_{m\mathbf{k}} \psi_{n'\mathbf{q}} \rangle, \quad (10)$$

where

$$\langle \psi_{n\mathbf{q}} \psi_{m\mathbf{k}} | W^c(\omega) | \psi_{m\mathbf{k}} \psi_{n'\mathbf{q}} \rangle = \int d\mathbf{r} d\mathbf{r}' \psi_{n\mathbf{q}}^*(\mathbf{r}) \psi_{m\mathbf{k}}^*(\mathbf{r}') W^c(\mathbf{r}\mathbf{r}'; \omega) \psi_{n'\mathbf{q}}(\mathbf{r}') \psi_{m\mathbf{k}}(\mathbf{r}). \quad (11)$$

Schematically, $W^c = vP^0v + vP^0vP^0v + \dots$ contains the screening from successive particle-hole excitations, each described by the mean-field polarization function, which in position representation reads

$$P^0(\mathbf{r}\mathbf{r}'; \omega) = 2 \sum_{kn} \sum_{k'n'} \psi_{n\mathbf{k}}^*(\mathbf{r}) \psi_{n'\mathbf{k}'}(\mathbf{r}) \psi_{n'\mathbf{k}'}^*(\mathbf{r}') \psi_{n\mathbf{k}}(\mathbf{r}') \times \left[\frac{n_{n\mathbf{k}}(1 - n_{n'\mathbf{k}'})}{\omega - E_{n'\mathbf{k}'} + E_{n\mathbf{k}} + i\delta} - \frac{n_{n'\mathbf{k}'}(1 - n_{n\mathbf{k}})}{\omega - E_{n'\mathbf{k}'} + E_{n\mathbf{k}} - i\delta} \right]. \quad (12)$$

Here, $n_{n\mathbf{k}}$ is the occupation of the state $\psi_{n\mathbf{k}}$ and the factor of 2 comes from summing over both spin channels. In this work, we perform a one-shot GW calculation. We therefore add a term $[\Delta\mu]\delta_{nn'}$ to Eq. (9) corresponding to a shift of the chemical potential, to ensure particle number conservation.

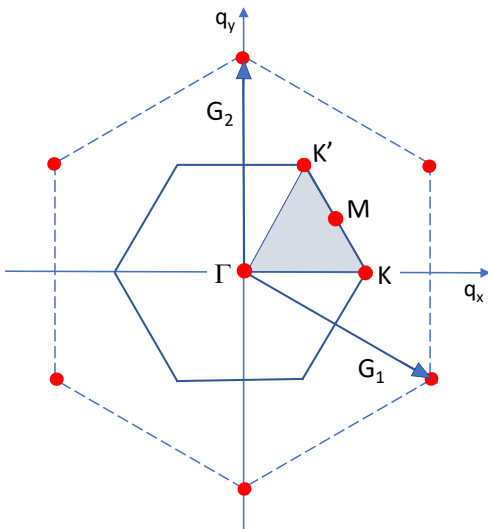


FIG. 2. The first Brillouin zone (enclosed by solid lines) for the 2D honeycomb lattice.

C. Computational Details

The most straightforward way to calculate the derivative of the Bloch functions which enters Eqs. (5)-(6), is to use the perturbation formula¹⁴

$$\left| \frac{\partial u_{n\mathbf{q}}}{\partial q_i} \right\rangle = \sum_{m \neq n} \frac{|u_{m\mathbf{q}}\rangle \langle u_{m\mathbf{q}} | \frac{\partial H(\mathbf{q})}{\partial q_i} | u_{n\mathbf{q}} \rangle}{E_{n\mathbf{q}} - E_{m\mathbf{q}}}, \quad (13)$$

equally valid for insulators as well as metals. This formula implies that $\langle \frac{\partial u_{n\mathbf{q}}}{\partial q_i} | u_{n'\mathbf{q}} \rangle = 0$ if $n' = n$. For real systems the sum over *all* bands can be tedious, however in tight-binding calculations for model systems the number of states are usually small.

For a topological insulator ($C \neq 0$) it is not possible to define a smooth and continuous gauge in the *whole* first BZ,⁴³ but since C is an observable it must be gauge invariant. The discontinuity can therefore be moved to the BZ boundary by a suitably chosen gauge. We have adopted a random gauge provided by the diagonalization routine used, where $u_{n\mathbf{q}}$ and $\frac{\partial u_{n\mathbf{q}}}{\partial q_i}$ have the same phase.

For the practical computation of $G_{nn'}^+(\mathbf{q})$ and its derivatives with respect to q_x and q_y we use the Matsubara formalism at low temperature with a 30×30 \mathbf{q} mesh. To converge the computation of M_{orb} (Eqs. (5)-(6)) we interpolate the Green's function and its derivatives to a non-uniform mesh which is particularly dense at the \mathbf{K} and \mathbf{K}' points (see Fig. 2). The results do not depend on whether the interpolation is linear or cubic.

From the static inverse Green's function it is straightforward to obtain the \mathbf{q} -resolved quasi-particle gap, $E_g(\mathbf{q})$, between the occupied and unoccupied bands at wavevector \mathbf{q} for the correlated system. In particular, we will present, together with M_{orb} , the Brillouin zone minimum and average gap, E_g^{min} and $\langle E_g \rangle$. The computation

of C requires a dense \mathbf{q} mesh in order to capture the singularity. We can still, with our 30×30 mesh, distinguish between the normal and topological insulating phases. In fact, the transition occurs when the gap closes, i.e. it can be traced by E_g^{min} .

IV. RESULTS

We will start by discussing the effect of the staggered potential, Δ_{AB} , on the orbital magnetization at complex hopping angle $\varphi = \pi/4$. Then, we study the effect of adding interactions, first with $\Delta_{\text{AB}} = 2$ and then with $\Delta_{\text{AB}} = 0$. For generality, we also present the magnetization in the plane of U and Δ_{AB} . Finally, the dependence of M_{orb} on φ is studied briefly. All results are obtained using $t_1 = 1$ and $t_2 = 1/3$, the same values used in the seminal paper by Thonhauser *et al.*¹²

A. Non-interacting case - Effect of varying Δ_{AB}

The Δ_{AB} -dependence of non-interacting M_{orb} is shown in Fig. 3 together with the minimum and Brillouin zone-averaged \mathbf{q} -resolved gaps, E_g^{min} and $\langle E_g \rangle$. The magnetization decreases monotonously and the average gap increases monotonously when increasing the strength of

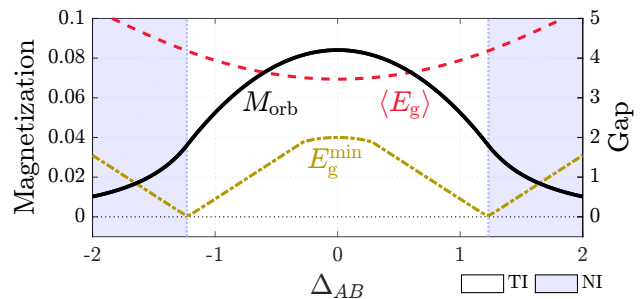


FIG. 3. Non-interacting M_{orb} , E_g^{min} and $\langle E_g \rangle$ as a function of Δ_{AB} . TI: topological insulator. NI: normal insulator.

the staggered potential, $|\Delta_{\text{AB}}|$. This can be understood from the expression

$$M_{\text{orb}} = -i \sum_{jk, n' \neq n} \epsilon_{zjk} \int_{\text{BZ}} \frac{d\mathbf{q}}{(2\pi)^2} (\epsilon_{n\mathbf{q}} + \epsilon_{n'\mathbf{q}}) \times \frac{\langle u_{n\mathbf{q}} | \frac{\partial H(\mathbf{q})}{\partial q_j} | u_{n'\mathbf{q}} \rangle \langle u_{n'\mathbf{q}} | \frac{\partial H(\mathbf{q})}{\partial q_k} | u_{n\mathbf{q}} \rangle}{(\epsilon_{n\mathbf{q}} - \epsilon_{n'\mathbf{q}})^2}, \quad (14)$$

which holds for non-interacting insulators, for which $G_{nn'}(\mathbf{q}) = i\delta_{n'n}f(E_{n\mathbf{q}})$ and $\partial G_{nn'}(\mathbf{q})/\partial q_i = 0$. Note that band n is occupied and n' unoccupied. The one-particle energy is measured relative to μ i.e $\epsilon_{n\mathbf{q}} = E_{n\mathbf{q}} - \mu$. If we imagine that the gap $E_g(\mathbf{q}) = E_{n'\mathbf{q}} - E_{n\mathbf{q}}$ is independent of \mathbf{q} and thus given by $\langle E_g \rangle$, then a small $\langle E_g \rangle$ implies a large M_{orb} and vice versa. This simplified

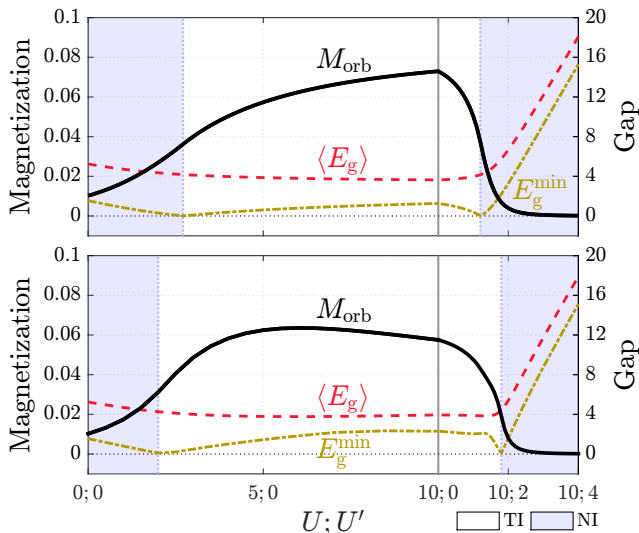


FIG. 4. M_{orb} , E_g^{min} and $\langle E_g \rangle$ as a function of U and U' with $\Delta_{\text{AB}} = 2$. Top: Hartree-Fock. Bottom: GW .

picture is useful if the inverse of $E_g(\mathbf{q})$ is only weakly \mathbf{q} dependent, which holds when we are far from phase transitions. The non-interacting value of M_{orb} at $\Delta_{\text{AB}} = 2$ matches the value of approximately 0.01 in an earlier work by Thonhauser *et al.*¹²

For small $|\Delta_{\text{AB}}|$, the system starts out as a topological insulator but at $|\Delta_{\text{AB}}| \approx 1.2$ a topological phase transition occurs and the system becomes a normal insulator, with $C = 0$. This transition is accompanied by the closing and reopening of the gap, E_g^{min} .

B. Effect of correlations with a non-zero Δ_{AB}

We now fix the staggered potential to $\Delta_{\text{AB}} = 2t_1 = 2$. M_{orb} is plotted in Fig. 4 versus the on-site and nearest-neighbor direct Coulomb integrals, U and U' , within the Hartree-Fock and GW approximation. As a complement to Fig. 4, we present M_{orb} in the two approximations in an overlay graph in Fig. 5.

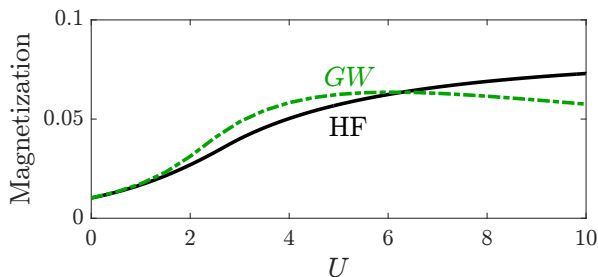


FIG. 5. Closer look on M_{orb} as a function of U within the Hartree-Fock and GW approximation. $\Delta_{\text{AB}} = 2$.

The HF results show that the mean-field effect of increasing U to infinity is to recover the non-interacting

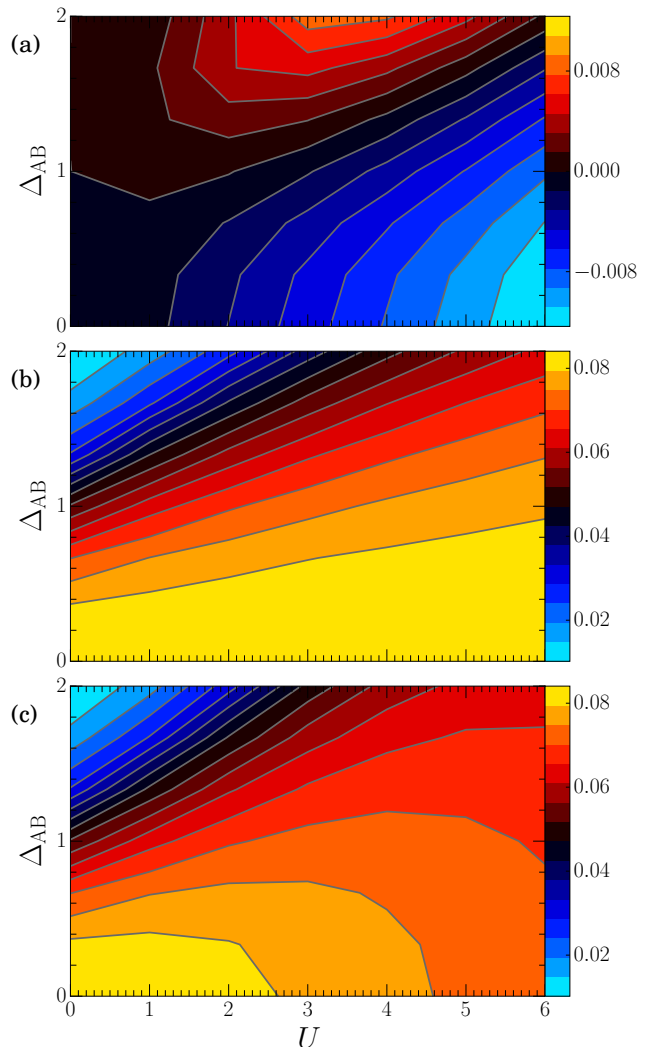


FIG. 6. The effect of correlations. (a) Difference between the GW and the Hartree-Fock magnetization. The correlation boost is clearly seen for large Δ_{AB} and intermediate U . (b) Hartree-Fock magnetization. (c) GW magnetization.

M_{orb} at $\Delta_{\text{AB}} = 0$ in Fig. 3, in other words, U counteracts the staggered potential. The effect of U' , which instead enhances it, is a decrease in M_{orb} .

The GW approximation yields a slightly larger M_{orb} than the Hartree-Fock approximation for small U . This increase originates from dynamical and non-local charge correlations, encompassed by the polarization function P , which makes the GW Green's function non-diagonal in the band index, n , when $U > 0$. The staggered potential, which modified the band energies $E_{n\mathbf{q}}$ that enter the polarization function, has a non-trivial effect on the self-energy. However, a slight decrease in the average gap, $\langle E_g \rangle$, can be observed compared to Hartree-Fock, which means that the charge fluctuations reduce the band gap. We have already noticed, in the non-interacting case, that a small band gap is associated with a large value of M_{orb} , but in the interacting case the entire dynamics has to be

considered for a complete understanding, since $G_{nn'}^+(\mathbf{q})$ is obtained by integrating over all frequencies in Eq. (8).

We have confirmed that the boost of the magnetization for small and intermediate U is caused by the last terms in Eq. (5) and (6) respectively, which are due to inter-band correlations ($n' \neq n$), with no non-interacting counterpart. Without these terms the magnetization would rapidly vanish when turning on the correlations. The correlation boost is seen in Fig. 6, where the difference between the *GW* and Hartree-Fock magnetization is displayed in the plane of U and Δ_{AB} together with the magnetization within each approximation. We see that the effect of correlations depends strongly on Δ_{AB} , and that boost occurs when the staggered potential dominates the nearest-neighbor hopping, i.e. when $\Delta_{AB} > 1$.

C. Effects of correlations with $\Delta_{AB} = 0$

Results analogous to those in Fig. 4 are presented in Fig. 7, with $\Delta_{AB} = 0$. Within the Hartree-Fock approximation, the magnetization is independent of U . This is because the staggered potential is absent, so the on-site repulsion yields the same constant energy shift to both bands. When increasing U' a sharp phase transition takes place after which M_{orb} decays rapidly. The reason for this sudden decrease of M_{orb} is seen in Fig. 8, where the occupation of sublattice A and B is plotted versus U and U' within the Hartree-Fock approximation, for $\Delta_{AB} = 0$. For a fixed value of $U = 10$, charge segregation occurs for a sufficiently large value of U' , after which all electrons very quickly end up occupying only sublattice B. This introduces a purely electronic counterpart of the ionic potential, Δ_{AB} , and naturally, the effect is a reduced M_{orb} .

Returning to Fig. 7, we see that in the *GW* approximation M_{orb} reduces with U , as opposed to the case $\Delta_{AB} = 2$ in Fig. 4. With $\Delta_{AB} = 0$, the mean-field potential vanishes (except for large values of U') and does therefore not affect the charge fluctuations. As mentioned before, the behavior of M_{orb} can not be completely understood in terms of the gap, but it is worth stressing that $\langle E_g \rangle$ indeed increases with U .

D. Effect of varying φ

The dependence of M_{orb} on the complex hopping phase φ is presented in Fig. 9 for $\Delta_{AB} = 2$ in the non-interacting limit and for $U = 5$, $U' = 0$ within the Hartree-Fock and the *GW* approximations. The curve for $U = 0$ is identical to Fig. 2 in Ref. 12 and displays a characteristic sinus-like φ dependence.^{12,13} This behavior survives in the interacting case in both approximations. Since the maximum value is obtained approximately at $\varphi = \pi/4$, independently of the interaction strength and the approximation, the M_{orb} presented in Fig. 3-7 can

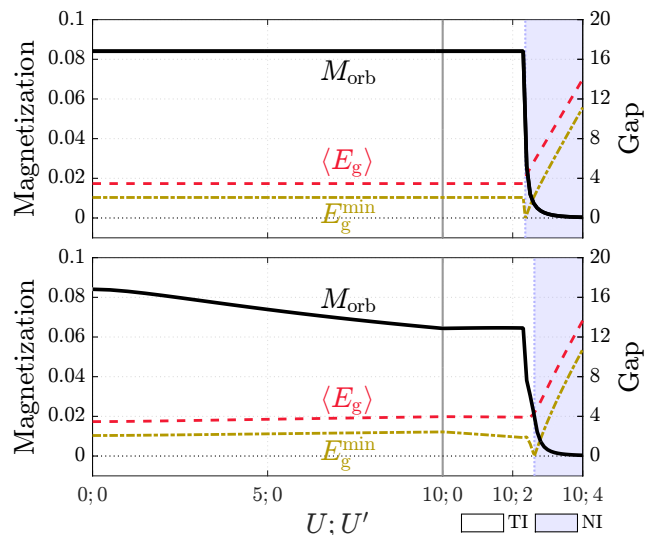


FIG. 7. M_{orb} , E_g^{min} and $\langle E_g \rangle$ as a function of U and U' with $\Delta_{AB} = 0$. Top: Hartree-Fock. Bottom: *GW*.

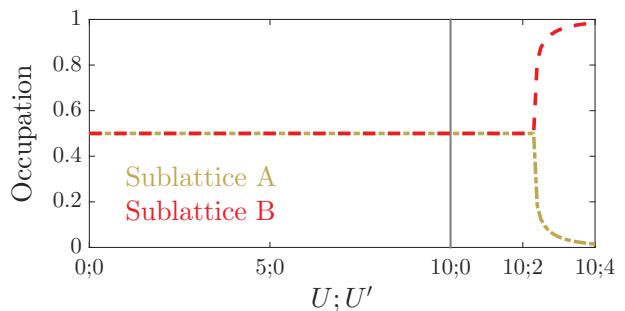


FIG. 8. Occupation of sublattice A and B as a function of U and U' within the Hartree-Fock approximation, with $\Delta_{AB} = 0$. Charge segregation occurs when U' exceeds a critical value.

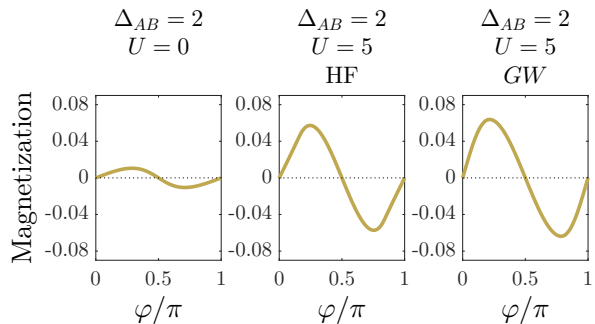


FIG. 9. M_{orb} as a function of the complex hopping phase φ . U' is set to zero.

be interpreted as the maximum possible magnetization for fixed Δ_{AB} , U and U' .

V. SUMMARY AND CONCLUSIONS

The effect of charge correlations on the orbital magnetization has been studied in the 2D Haldane-Hubbard model by adding the GW self-energy. To the best of our knowledge, this is the first study on orbital magnetization where the screening has been treated microscopically. Qualitatively, we are lead to distinguish between two quite different situations.

(i) When the staggered potential dominates the nearest-neighbor hopping we find that the main effect of GW correlations, for small values of the the on-site U and vanishing U' , is an increase of the orbital magnetization compared to the Hartree-Fock approximation. In fact, the non-interacting modern theory of orbital magnetization is known to underestimate M_{orb} in materials outside the realm of the Haldane-Hubbard model, such as ferromagnetic transition metals. The explanation is hidden in the frequency-integral of Eq. (8), which depends on the entire dynamics, in particular, both the renormalization of the two bands, as well as the gap. In the

non-interacting limit, the correlation boost of M_{orb} can be understood mainly from the narrowing of the quasi-particle gap, using Eq. (14).²³

(ii) When the nearest-neighbor hopping dominates the staggered potential, the GW correlations are instead found to yield a decrease in the magnetization for small values of U and vanishing U' . For $\Delta_{\text{AB}} = 0$, inversion symmetry is recovered and the polarization function used to calculate the Green's function within the one-shot GW approximation becomes independent of U . For large enough values of U' , charge segregation sets in, resulting in a purely electronic equivalent of the staggered potential which breaks inversion symmetry, resulting in a drop in M_{orb} both within the Hartree-Fock and the GW approximation.

ACKNOWLEDGMENTS

This work was supported by the Swedish Research Council VR (T. J. Sjöstrand and F. Aryasetiawan). One of us (K. Karlsson) would like to thank J. Kanski for fruitful discussions.

-
- ¹ O. Hjortstam, K. Baberschke, J. M. Wills, B. Johansson, and O. Eriksson, *Phys. Rev. B* **55**, 15026 (1997).
- ² Daisuke Kan, Masaichiro Mizumaki, Tomoe Nishimura, and Yuichi Shimakawa, *Phys. Rev. B* **94**, 214420 (2016).
- ³ Martin A. Schoen, Juriaan Lucassen, Hans T. Nembach, T. J. Silva, Bert Koopmans, Christian H. Bach, and Justin M. Shaw, *Phys. Rev. B* **95**, 134410 (2017).
- ⁴ Z. Wang and P. Zhang, *Phys. Rev. B* **76**, 064406 (2007).
- ⁵ A. Malashevich, I. Souza, S. Coh, and D. Vanderbilt, *New Journal of Physics*, **12**, 053032 (2010).
- ⁶ A. M. Essin, J. E. Moore, and D. Vanderbilt, *Phys. Rev. Lett.* **102**, 146805 (2009).
- ⁷ A. M. Essin, A. M. Turner, J. E. Moore, and D. Vanderbilt, *Phys. Rev. B* **81**, 205104 (2010).
- ⁸ S. Murakami, *Phys. Rev. Lett.* **97**, 236805 (2006).
- ⁹ D. Xiao, W. Yao, and Q. Niu, *Phys. Rev. Lett.* **99**, 236809 (2007).
- ¹⁰ D. Xiao, Y. Yao, Z. Fang, and Q. Niu, *Phys. Rev. Lett.* **97**, 026603 (2006).
- ¹¹ F. Wilhelm, J. P. Sanchez, J. P. Brison, D. Aoki, A. B. Shick, and A. Rogalev, *Phys. Rev. B* **95**, 235147 (2017).
- ¹² T. Thonhauser, D. Ceresoli, D. Vanderbilt, and R. Resta, *Phys. Rev. Lett.* **95**, 137205 (2005).
- ¹³ T. Thonhauser and D. Vanderbilt, *Phys. Rev. B* **74**, 235111 (2006).
- ¹⁴ D. Ceresoli, T. Thonhauser, D. Vanderbilt, and R. Resta, *Phys. Rev. B* **74**, 024408 (2006).
- ¹⁵ D. Xiao, J. Shi, and Q. Niu, *Phys. Rev. Lett.* **95**, 137204 (2005).
- ¹⁶ R. Resta, *Phys. Rev. Lett.* **80**, 1800 (1998).
- ¹⁷ R. Resta, D. Ceresoli, T. Thonhauser, and D. Vanderbilt, *ChemPhysChem* **6**, 1815 (2005).
- ¹⁸ R. Resta, *J. Phys.: Condens. Matt.* **22**, 123201 (2010).
- ¹⁹ J. Shi, G. Vignale, D. Xiao, and Q. Niu, *Phys. Rev. Lett.* **99**, 197202 (2007).
- ²⁰ T. Thonhauser, *Int. J. Mod. Phys. B* **25**, 1429 (2011).
- ²¹ D. Xiao, M.-C. Chang, and Q. Niu, *Rev. Mod. Phys.* **82**, 1959 (2010).
- ²² M. G. Lopez, D. Vanderbilt, T. Thonhauser and I. Souza, *Phys. Rev. B* **85**, 014435 (2012).
- ²³ D. Ceresoli, U. Gerstmann, A. P. Seitsonen, and F. Mauri, *Phys. Rev. B* **81**, 060409(R) (2010).
- ²⁴ J. P. Hanke, F. Freimuth, A. K. Nandy, H. Zhang, S. Blügel, and Y. Mokrousov, *Phys. Rev. B* **94**, 121114(R) (2016).
- ²⁵ S. A. Nikolaev and I. V. Solov'yev, *Phys. Rev. B* **89**, 064428 (2014).
- ²⁶ I. M. Miron, K. Garello, G. Gaudin, P. Zermatten, M. V. Costache, S. Auffret, S. Bandiera, B. Rodmacq, A. Schuhl, and P. Gambardella, *Nature (London)* **476**, 189 (2011).
- ²⁷ S. Heinze, K. von Bergmann, M. Menzel, J. Brede, A. Kubetzka, R. Wiesendanger, G. Bihlmayer, and S. Blügel, *Nat. Phys.* **7**, 713 (2011).
- ²⁸ Y. Taguchi, Y. Oohara, H. Yoshizawa, N. Nagaosa, and Y. Tokura, *Science* **291**, 2573 (2001).
- ²⁹ R. Nourafkan, G. Kotliar, and A. M. S. Tremblay, *Phys. Rev. B* **90**, 125132 (2014).
- ³⁰ F. Aryasetiawan and K. Karlsson, *Journal of Physics and Chemistry of Solids*, 1-22, (2017).
- ³¹ F. Aryasetiawan, K. Karlsson, and T. Miyake, *Phys. Rev. B* **93**, 161104(R) (2016).
- ³² L. Hedin, *Phys. Rev.* **139**, A796 (1965).(216)
- ³³ A. Georges, G. Kotliar, W. Krauth, and M. J. Rozenberg, *Rev. Mod. Phys.* **68**, 13 (1996).
- ³⁴ S. Biermann, F. Aryasetiawan, and A. Georges, *Phys. Rev. Lett.* **90**, 086402 (2003).
- ³⁵ F. D. M. Haldane, *Phys. Rev. Lett.* **61**, 2015 (1988).
- ³⁶ C. L. Kane and E. J. Mele, *Phys. Rev. Lett.* **95**, 146802

- (2005); **95**, 226801 (2005).
- ³⁷ K. v. Klitzing, G. Dorda, and M. Pepper, Phys. Rev. Lett **45**, 494 (1980).
- ³⁸ G. Jotzu, M. Messer, R. Desbuquois, M. Lebrat, T. Uehlinger, D. Greif, and T. Esslinger, Nature (London) **515**, 237-240 (2014); arXiv:1406.7874v2.
- ³⁹ L. Ci, L. Song, C. Jin, D. Jariwala, D. Wu, Y. Li, A. Srivastava, Z. F. Wang, K. Storr, L. Balicas, F. Liu and P. M. Ajayan, Nature Materials, **9**, 430 (2010).
- ⁴⁰ F. Aryasetiawan, M. Imada, A. Georges, G. Kotliar, S. Biermann, and A. I. Lichtenstein, Phys. Rev. B **70**, 195104 (2004).
- ⁴¹ T. O. Wehling, E. Sasioglu, C. Friedrich, A. I. Lichtenstein, M. I. Katsnelson, and S. Blügel, Phys. Rev. Lett. **106**, 236805 (2011).
- ⁴² T. I. Vanhala, T. Siro, L. Liang, M. Troyer, A. Harju, and P. Törmä, Phys. Rev. Lett. **116**, 225305 (2016).
- ⁴³ A. A. Soluyanov and D. Vanderbilt, Phys. Rev. B **85**, 115415 (2012).